Realization of quantum discrete Fourier transform with NMR

FANG Ximing[1,2], ZHU Xiwen[1], FENG Mang[1], MAO Xi'an[1] & DU Fei[1]

1. State Key Laboratory of Magnetic Resonance and Atomic and Molecular Physics, Wuhan Institute of Physics and Mathematics, Chinese Academy of Sciences, Wuhan 430071, China;
2. Department of Physics, Hunan Normal University, Changsha 410081, China
Correspondence should be addressed to Zhu Xiwen (e-mail: xwzhu@nmr.whcnc.ac.cn).

Abstract The pulse sequences of the logic operations used in quantum discrete Fourier transform are designed for the experiment of nuclear magnetic resonance(NMR), and 2-qubit discrete Fourier transforms are implemented experimentally with NMR. The experimental errors are examined and methods for reducing the errors are proposed.

Keywords: quantum computation, quantum discrete Fourier transform (QDFT), nuclear magnetic resonance.

Quantum discrete Fourier transform (QDFT) algorithm[1,2] originally stemmed from the classical fast Fourier transform. It played a key role in many quantum algorithms (such as Shor's factoring algorithm[3] and discrete logarithm[3]) and in the preparation of pseudo-pure states[4]. The application of quantum computation to mimic quantum chaos proposed by Schack[5] and Brun[6] was also based on QDFT. Therefore, it is significant to find out how to realize QDFT. Recently, Pravia et al.[1)] reported their experiment in QDFT with the spectroscopy of NMR, but they did not present the results quantitatively. In this contribution, we will report the quantitative results of the experimental implementation of 2-qubit QDFT and discuss the errors in the experiments. Then we will propose some methods for reducing errors.

For an arbitrary positive integer a, there exist positive integers c, q and l, where $0 < (a, c) < q$, and $q=2^l$. The QDFT of the state $|a\rangle$ is defined as:

$$\mathrm{QDFT}|a\rangle = \frac{1}{\sqrt{q}} \sum_{c=0}^{q-1} |c\rangle \exp\{i2\pi ac/q\}. \tag{1}$$

According to Ekert et al.[2], the basic QDFT is composed both of the Hadamard transform R_i of a single qubit i and of the controlled phase shift transformation $S_{j,k}$ of the two qubits, whose matrices are

$$R_i = \frac{1}{\sqrt{2}} \begin{pmatrix} 1 & 1 \\ 1 & -1 \end{pmatrix}, \tag{2}$$

$$S_{j,k} = \begin{pmatrix} 1 & 0 & 0 & 0 \\ 0 & 1 & 0 & 0 \\ 0 & 0 & 1 & 0 \\ 0 & 0 & 0 & e^{i\theta_{j,k}} \end{pmatrix}, \tag{3}$$

where $\theta_{j,k} = \frac{\pi}{2^{k-j}}$, k labels the control qubit, j the target qubit and $k > j$. R_i makes the single qubit i from $|0\rangle_i$ and $|1\rangle_i$ the superpositions $(|0\rangle_i + |1\rangle_i)/\sqrt{2}$ and $(|0\rangle_i - |1\rangle_i)/\sqrt{2}$, respectively. $S_{j,k}$ will add a rotating phase $e^{i\theta_{j,k}}$ to the state $|11\rangle_{j,k}$, and the other three states of the two qubits remain unchanged under $S_{j,k}$.

The last operation in QDFT is the exchange of the positions of the higher and lower qubits, denoted by $SW_{i,j}$. If the results of QDFT are the final outputs of the whole quantum computing, the operation of $SW_{i,j}$ can be simply replaced by inversely reading results of the output qubits. Otherwise, $SW_{i,j}$ must be executed. The matrix of $SW_{i,j}$ is

1) Pravia, M. et al., Observations of quantum dynamics by solution-state NMR spectroscopy, e-print, quant-ph/9905061.

$$SW_{i,j} = \begin{pmatrix} 1 & 0 & 0 & 0 \\ 0 & 0 & 1 & 0 \\ 0 & 1 & 0 & 0 \\ 0 & 0 & 0 & 1 \end{pmatrix}. \quad (4)$$

Obviously, $SW_{i,j}$ will result in a swapping of the two qubits i and j, that is, $|\varepsilon_i \varepsilon_j\rangle \rightarrow |\varepsilon_j \varepsilon_i\rangle$, in which $\varepsilon_i, \varepsilon_j \in \{0,1\}$.

The three operations above can be carried out in NMR with following pulse sequences:

$$PR_i = X_i(\pi) Y_i\left(-\frac{\pi}{2}\right), \quad PS_{j,k} = Z_j\left(-\frac{\pi}{4}\right) Z_k\left(-\frac{\pi}{4}\right) J_{j,k}\left(\frac{\pi}{2}\right)$$

and

$$PSW_{i,j} = X_i\left(\frac{\pi}{2}\right) Y_i\left(-\frac{\pi}{2}\right) J_{i,j}(-\pi) X_i\left(-\frac{\pi}{2}\right) Y_i\left(\frac{\pi}{2}\right) Y_j\left(-\frac{\pi}{2}\right) X_j\left(-\frac{\pi}{2}\right) J_{i,j}(-\pi) Y_j\left(\frac{\pi}{2}\right) X_j\left(\frac{\pi}{2}\right) X_i\left(\frac{\pi}{2}\right)$$
$$\cdot Y_i\left(-\frac{\pi}{2}\right) Y_j\left(\frac{\pi}{2}\right) X_j\left(\frac{\pi}{2}\right) Y_j\left(-\frac{\pi}{2}\right) J_{i,j}(-\pi) Y_i\left(\frac{\pi}{2}\right),$$

where X, Y and Z represent the rotation axes and $J_{i,j}$ the two-nucleus rotation around Z, and the rotating angles are written in the parentheses. It must be pointed out that phase differences $e^{i\frac{\pi}{2}}$, $e^{-i\frac{\theta_{k-j}}{4}}$ and $e^{-i\frac{3}{4}\pi}$ exist between the pulse sequences PR_i, $PS_{j,k}$ and $PSW_{i,j}$ and the corresponding logic operations (2)—(4) respectively. However, as the state space of whole system expands with the tensor product of the qubits subsystems, the phases caused by the operations to any qubit at any time are the common phases of the whole system. Therefore, there are no actual differences between pulse sequences mentioned above and the logic operations (2)—(4), respectively.

Two experiments of 2-qubit QDFT were implemented. We chose ^{1}H and ^{13}C in the molecule of carbon-13 labeled chloroform $^{13}CHCl_3$ (Cambridge Isotope Laboratories, Inc.) as the two-spin systems in the experiments and d6-acetone as the solvent, with the solute/solvent ratio being 1:1 (v/v). Spectra were recorded on a Bruker ARX 500 spectrometer with a probe tuned at 500.13 MHz for ^{1}H and at 125.77 MHz for ^{13}C.

The Hamiltonian of the system can be written as

$$H = \omega^H I_z^H + \omega^C I_z^C + 2\pi \hbar J I_z^H I_z^C + H_{env}, \quad (5)$$

where I^H_Z and I^C_Z represent operators of Z components of nuclear spins of ^{1}H and ^{13}C, ω^H and ω^C are the level splittings of nuclei ^{1}H and ^{13}C in the static magnetic field and RF field, and J denotes the spin-spin coupling strength of the above two nuclei. Therefore, the first and the second terms of eq. (5) represent the interaction of the two spins with the static magnetic and RF field respectively. The third term shows spin-spin interaction. The last term is the coupling between the system and environment, which can be omitted because it is so small that it can be ignored.

The logic circuit of 2-qubit QDFT is shown in fig. 1(a). As the actual pulses are imperfect, errors can always be made in the experiments. Therefore, we have to reduce the number of pulse sequences to decrease the experimental errors, which can also help

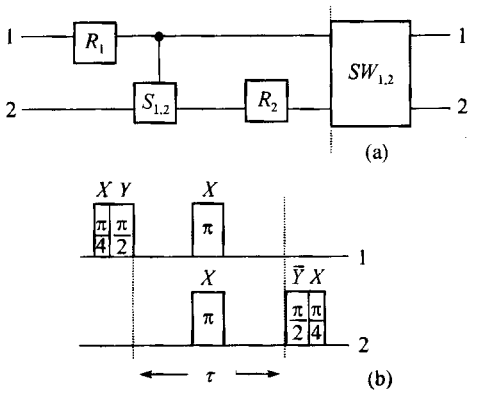

Fig. 1. The logic circuit of two-qubit quantum discrete Fourier transform (a) and the NMR pulse sequences corresponding to operations $R_1 S_{1,2} R_1$ (b). X and Y denote the direction of the pulses, the bars over the alphabet denote the opposite direction of the axis. The numbers in the boxes denote the angle of the pulses. $\tau = 1/4J$ is the evolution time.

to minimize the effect of decoherence. The reduced pulse sequences of the operations $R_1S_{1,2}R_1$ used in the experiments are shown in fig. 1(b). From the operations (fig. 1(a)) or the combination of the reduced operations $R_1S_{1,2}R_1$ with SW (fig. 1(b)), we can derive the matrix of QDFT as follows:

$$\mathrm{QDFT} = \begin{pmatrix} 1 & 1 & 1 & 1 \\ 1 & i & -1 & -i \\ 1 & -1 & 1 & -1 \\ 1 & -i & -1 & i \end{pmatrix} \equiv \mathrm{F}. \tag{6}$$

The experiments were carried out as follows. First, the effective pure states $|01\rangle$ and $|11\rangle$ were prepared by temporal averaging, followed by the implementation of the pulse sequences of $R_1S_{1,2}R_1$ and SW. At last, the density matrix was reconstructed by the technique of state tomography for obtaining the measured elements. We show in fig. 2 the experimental and theoretical results of the QDFT of the state $|01\rangle$, where the real and imaginary parts of the density matrices $F|01\rangle\langle 01|F^+$ are demonstrated in fig. 2(a), (b), (c) and (d), respectively. The corresponding results for the state $|11\rangle$ after QDFT is shown in

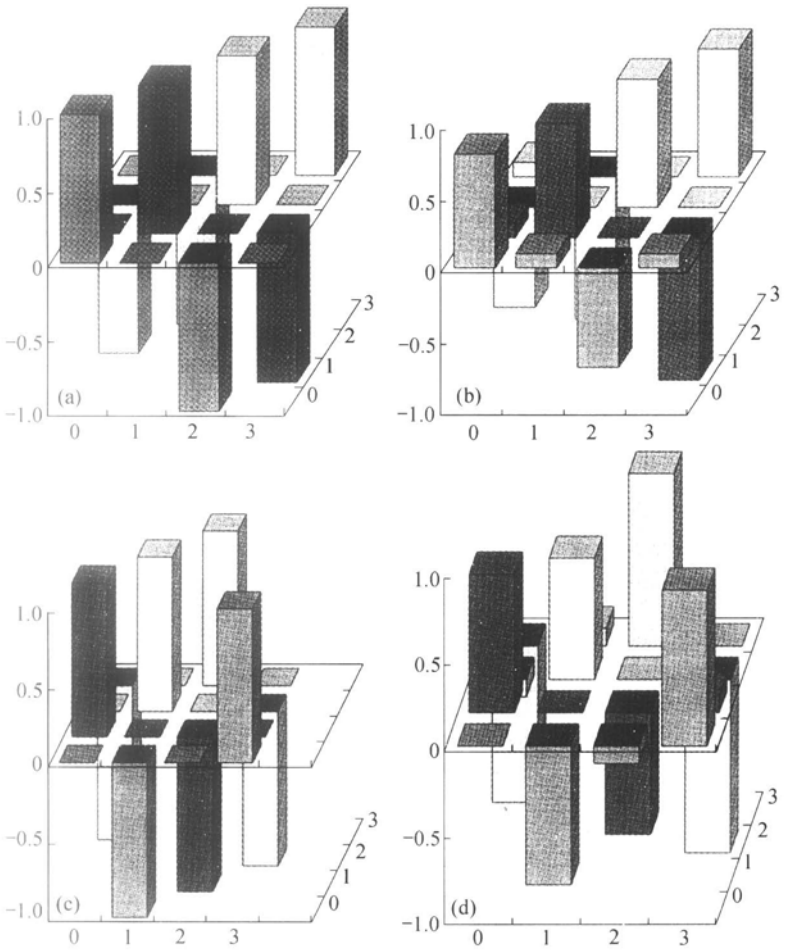

Fig. 2. The distribution of the density matrix $|01\rangle\langle 01|$ after QDFT. The axes in the horizontal plane denote the elements in the matrix, 0, 1, 2 and 3 correspond to states $|00\rangle$, $|01\rangle$, $|10\rangle$ and $|11\rangle$, respectively. The vertical axis denotes the magnitude of the elements. (a) and (b) represent the real parts of the theoretically expected and experimentally measured density matrix, (c) and (d) the imaginary ones, respectively.

fig. 3. It can be found in these figures that the experimental and the theoretical results are in good agreement, which shows the applicability of the NMR implementation of the QDFT. Meanwhile, it can be also found that the errors of the non-diagonal elements are larger than those of the diagonal, in which the largest error is about 20%. In our opinion, the errors in the experiments were caused by the following sources. Firstly, the off-diagonal elements are very sensitive to the imperfection of $\frac{\pi}{2}$ pulses, which made the errors of the off-diagonal elements larger than the diagonal. In our experiments we tried to reduce the effect of the imperfection of π pulses without using the technique of phase cycling reducing the effects of the imperfection of $\frac{\pi}{2}$ pulses. The second sources of errors are the inhomogeneity of the static magnetic field and RF field, and the inhomogeneity of the decay signal during the experiments. In addition, the inaccurate calibration of the initial time in treating the spectra may also cause errors. As the initial time in our experiments was set by the standard phase technique, the calibration errors of the initial time were large, which would lead to much larger errors of the final results due to the oscillation of off-diagonal elements. Therefore, it would be an important task for the future quantum computing experiment with NMR to make the pulses accurately, and the RF field and the statistic magnetic field homogeneously. It is very important to find methods for calibrating the initial time accurately or for developing softwares to reduce the errors of the initial time.

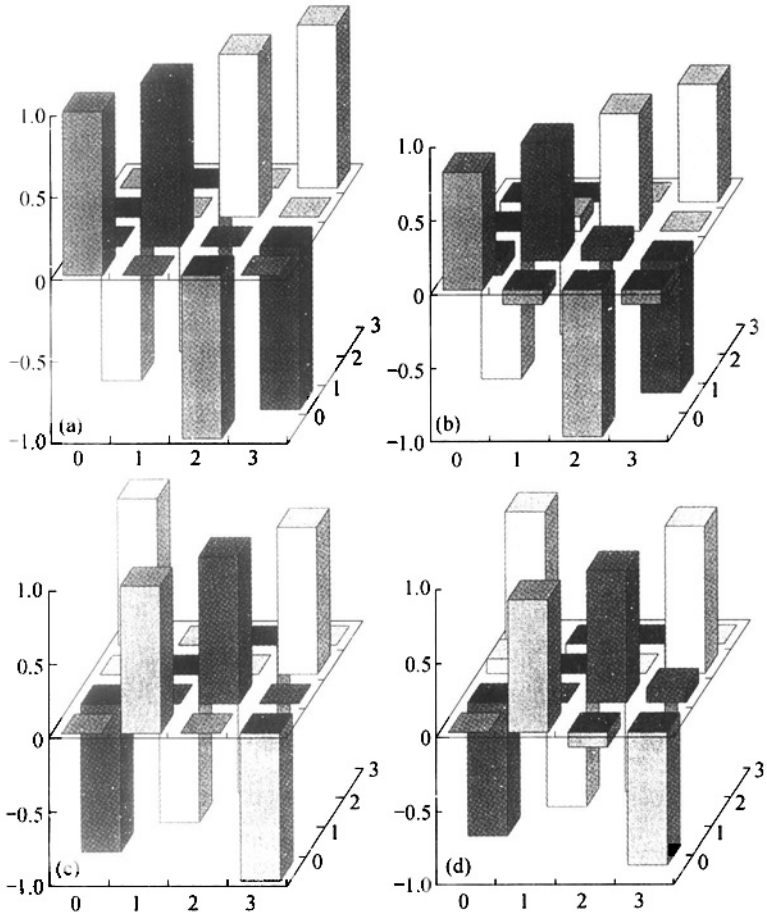

Fig. 3. The distribution of the density matrix $|11\rangle\langle 11|$ after QDFT. The meaning of the symbols in this figure is the same as in fig. 2.

Acknowledgements This work was supported by the Chinese Academy of Sciences and the National Natural Science Foundation of China (Grant No.19734060).

References

1. Coppersmith, D., An approximate Fourier transform useful in quantum factoring, IBM Research Report, 1994, No.RC 19642.
2. Ekert, A., Jozsa, R., Quantum computation and Shor's factoring algorithm, Rev. Mod. Phys., 1996, 68: 733.
3. Shor, W., Algorithm for quantum computation: discrete logarithms and factoring, in Proceedings of in 35th Annual Symposium on Foundations of Computer Science, Los Alamitos, CA. IEEE Computer Society Press, 1994, 124.
4. Chuang, I. L., Gershenfeld, N., Kubinec, M. G. et al., Bulk quantum computation with nuclear magnetic resonance: theory and experiment, Proc. R. Soc. Lond. A, 1998, 454: 447.
5. Schack, R., Using a quantum computer to investigate quantum chaos, Phys. Rev. A., 1998, 57: 1634.
6. Brun, T. A., Schack, R., Realizing the quantum Baker's map on a NMR quantum computer, Phys. Rev. A., 1999, 59: 2649.

(Received November 17, 1999; accepted December 21, 1999)